Review of Catalyst Materials and Catalytic Steam Reforming Reactions in SOFC Anodes

Andersson, Martin; Paradis, Hedvig; Yuan, Jinliang; Sundén, Bengt

Published in:
International Journal of Energy Research

DOI:
10.1002/er.1875

2011

Review of Catalyst Materials and Catalytic Steam Reforming Reactions in SOFC Anodes

Martin Andersson *Hedvig Paradis*
Department of Energy Sciences, Faculty of Engineering,
Lund University, Box 118, 221 00 Lund, Sweden

Jinliang Yuan *Bengt Sundén*
Department of Energy Sciences, Faculty of Engineering,
Lund University, Box 118, 221 00 Lund, Sweden

Corresponding Author: Martin.Andersson@energy.lth.se

Abstract

It is expected that fuel cells will play a significant role in a future sustainable energy system, due to their high energy efficiency and possibility to use renewable fuels. Fuels, such as biogas, can be produced locally close to the customers. The improvement for fuel cells during the last years has been fast, but the technology is still in the early phases of development, however the potential is enormous.

The reforming reaction of hydrocarbons (e.g., methane) is a key one for an effective solid oxide fuel cell (SOFC) operation. This reaction could either be described by global kinetics or by elementary surface reaction kinetics. When a global approach is applied, the reaction rates depend on temperature, partial pressures, activation energy and the pre-exponential factor. Note that the last two mentioned parameters are normally calculated from experimental data. Different detailed reaction mechanisms (considering elementary surface kinetics) are developed, but there is a disagreement considering the involved reaction pathways, rate-limiting steps and intermediate species. It is found that detailed kinetics of the reforming reaction is important for design and development of new effective catalytic materials. A thermodynamical analysis tells that nickel and ruthenium are suitable catalytic materials for the methane steam reforming reactions.

Keywords: SOFC, Internal reforming, Catalytic activity, Reaction pathway

1 Introduction

Fuel cells directly convert the free energy of a chemical reactant to electrical energy and heat. This is different from a conventional thermal power engine, where the fuel is oxidized in a combustion process combined with a conversion process (thermal-mechanical-electrical energy), that takes place after the combustion. If pure hydrogen is used, no pollution of air and environment occurs at all, because the output from the fuel cells is electricity, heat and water. Fuel cells do not store energy as batteries do [1].The fuel cell is not a new invention, since the electrochemical process was discovered already in 1838-39. The interest in fuel cells has been growing exponentially, which is evident from the amount of published scientific papers, after year 2000 [2]. Among various types of fuel cells (FCs), the solid oxide fuel cell (SOFC) has attained significant interest due to its high efficiency and low emissions of pollutants to the environment. High temperature operation offers SOFC many advantages, such as high electrochemical reaction rate, flexibility of using various fuels and toleration of impurities [3].

The SOFC electrolyte is non porous ceramic, normally Y_2O_3 stabilized ZrO_2 (YSZ). At an operating temperature between 600-1000 °C, the ceramic electrolyte becomes non-conductive for

electrons, but conductive to oxygen ions. Cathodes are mostly made from electronically conducting oxides or mixed electronically conducting and ion-conduction ceramics. The anode consists normally of nickel/yttria stabilized zirconia (Ni/YSZ) cermet. SOFCs can be designed with planar, tubular or monolithic structures. The planar design is normally more compact, compared to the tubular one, i.e., a higher volume of specific power is achieved. Tubular and planar SOFCs can be either electrolyte-, anode-, cathode- or metal- supported. An electrolyte-supported SOFC has thin anode and cathode (~50 μm), and the thickness of the electrolyte is more than 100 μm. This design works preferably at temperatures around 1000 °C. In an electrode-supported SOFC either the anode or the cathode is thick enough to serve as the supporting substrate for cell fabrication, normally between 0.3 and 1.5 mm. The electrolyte is in this configuration very thin, and the operating temperature can be reduced to an intermediate temperature (IT), i.e. 600-800 °C [4].

SOFCs can work with a variety of fuels, e.g., hydrogen, carbon monoxide, methane and combinations of these [5-6]. Oxygen is reduced in the cathode (Eq.(1)). The oxygen ions are transported through the electrolyte, but the electrons are prevented to pass through the electrolyte. The electrochemical reactions (Eqs.(2)-(3)) take place at the anodic three-phase boundary (TPB). Methane needs to be reformed (Eq.(4)) before the electrochemical reactions [7]. Carbon monoxide can be oxidized in the electrochemical reaction (Eq. (3)) but can also react with water (Eq.(5)). The reactions described here are the overall reactions, more detailed reaction mechanisms can be found in [7]. Note that methane is not participating in the electrochemical reactions at the anodic TPB, but catalytically converted, within the anode, into carbon monoxide and hydrogen. Hydrogen and carbon monoxide are used as fuel in the electrochemical reactions [6].

$$O_2 + 4e^- \Leftrightarrow 2O^{2-} \tag{1}$$

$$H_2 + O^{2-} \Leftrightarrow H_2O + 2e^- \tag{2}$$

$$CO + O^{2-} \Leftrightarrow CO_2 + 2e^- \tag{3}$$

$$CH_4 + H_2O \Leftrightarrow 3H_2 + CO \tag{4}$$

$$CO + H_2O \Leftrightarrow H_2 + CO_2 \tag{5}$$

The aim of this work is to review the state-of-the-art concerning modeling of the methane reforming reactions, that occurs within a SOFC. Global kinetic approaches as well as elementary surface reaction kinetics are studied. Metals suitable for catalysis of the methane steam reforming reactions are compared. Different reaction mechanisms, including comparison of surface coverages, are outlined and discussed.

2 Internal reforming reactions

The reforming reactions (Eqs. (4)-(5)) in SOFC systems can be conducted both externally and internally. The external reforming (ER), such as the pre-reformer in a SOFC system, means that the reformer is placed outside the cell, which is possible for all types of fuel cells. The internal reforming (IR) means that the reforming reactions occurr within the cell. A pre-reformer needs extra steam, since it can not directly use the steam generated in the electrochemical reactions. The IR can be direct or indirect. In the direct internal reforming (DIR) approach, the reforming processes occur together with the electrochemical reactions within the anode. In the indirect internal reforming (IIR) approach the reforming reactions appear in a reformer (within the cell) in close contact with the anode where the exothermic electrochemical reactions take place. The IR reactions decrease the requirement for cell cooling (less surplus of air). Less steam is needed and finally it offers advantages with respect to the capital cost. Up to half of the heat produced by the oxidation reaction

could be “consumed” by the steam reforming process. This would improve the system electrical efficiency [8-9].

The probability for carbon depositions depends on the steam-to-carbon ratio. It has been well established that the key reactions occur over a surface layer of nickel particles. If a layer of carbon is allowed to build up and attach to a nickel crystallite rapid catalyst breakdown can occur, due to the graphite formation. It should be noted that hydrocarbons with a longer carbon chain than methane have a higher propensity for carbon deposition [10]. The risk of carbon deposition can be decreased if pre-reforming is carried out before the cell, or changes can be made to the anode structure [11]:

- Complete or partial replacement of doped zirconia with doped ceria or ceria-zirconia possessing a higher lattice oxygen reactivity/mobility. This can be combined with complete or partial replacement of Ni by Cu.
- Replacement of doped zirconia by complex perovskites with their doping by metals active in the steam reforming reaction.
- Complete or partial replacement of Ni by precious metals in cermets with complex perovskites or doped zirconia as oxide phases.

In a conventional high temperature (HT) SOFC the endothermic steam reforming reaction is very fast. This can result in a temperature drop at the inlet of the stack. The temperature gradient results in thermal tensions, which in the worst case causes mechanical failure of the cells [8]. The problem of the tensions and big temperature gradients close to the inlet region could be solved with different approaches:

- Lowering the operating temperature to an intermediate range to reduce the steam reforming reaction rates [12].
- Recycling a part of the anode gas to obtain a dilution of the fuel. The rate of reforming reactions decreases, due to decrease in fuel concentration. A 50 percent recycling results in sufficient steam for the reforming reactions and the cost for a separate water supply is saved as well [8].
- The anode material can be designed with the aim of a decreased steam reforming activity. Until now these new SOFC materials, such as iron or copper, have too low electronic conductivity to meet the real world requirements. When nickel is replaced during the fabrication process with for example iron, a less catalytic active anode regarding the reforming activity is constructed. This is in the short term a promising method based on well-established production processes. Other researches replaced nickel with copper and the same effect has been reached [8].

3 Global reaction kinetics

Several kinetic expressions considering the steam reforming reaction are developed in the literature. The reaction order varies significantly between the schemes, in terms of orders of methane and water (m and n in Eq.(6)), see [1] for typical values. The reaction order of methane (m) varies between 0.85 and 1.4. For water both negative and positive values for reaction order (n) exist. However, it has been shown that all these findings could be correct for the chosen operating conditions of the experiments. A small steam-to-carbon (SC) ratio gives positive reaction order of water. SC in the order of 2 yields the reaction orders of water close to zero, and high SC gives negative values [13]. Experimental work has shown that it is possible to change the steam reforming reaction orders by modifying the anode, for example m increased from 0.85 to 1.4 and n

decreased from -0,35 to -0,8 when other compounds are added to Ni-YSZ anode [12]. As seen in [1], comparison with experimental data is rare, but it is worthwhile to note that the reaction orders (*m* and *n*) usually originate from fitting experimental data to a kinetic expression.

$$r_{r,Arr} = k \cdot p_{CH_4}^{m} \cdot p_{H_2O}^{n} \cdot \exp\left(\frac{-E_a}{\mathrm{R} \cdot T}\right) \tag{6}$$

where r_r is the reaction rate of steam reforming reaction, p the partial pressure, R the ideal gas constant and T the temperature. The unit for the reaction rate is dependent on the pre-exponential factor. Normally the unit for the methane steam reforming reaction rate is in mol/(s·m^2), and can then be converted to mol/(s·m^3) after multiplying it with the active surface area to volume ratio (*AV,* in m^2/m^3). The range for the AV (related to catalytic kinetic reactions) varies in the literature between $1 \cdot 10^5$ m^2/m^3 [14] and $2.2 \cdot 10^6$ m^2/m^3 [15] for SOFC anodes. For example, the measured surface area to volume ratio for Ni/YSZ material developed for SOFC anodes (with a pore size of 225 nm) is $70 \cdot 10^6$ m^2/m^3 [16]. Note that not all the surfaces are available for catalytic reactions, due to the distribution of catalyst, non available pores and mass transfer limitations among others. An AV of $2.2 \cdot 10^6$ m^2/m^3 corresponds to 3.1 percent of the total Ni/YSZ surface area in this specific case. The kinetic expression for the methane steam reforming in Eq.(6) is of Arrhenius type, and can be compared to an expression of the Langmuir- Hinshelwood type, as shown in Eq. (7) [17]:

$$r_{r,Lang.} = k \cdot \frac{p_{CH_4} \cdot p_{H_2O} \cdot K_{CH_4} \cdot K_{H_2O}}{\left(1 + p_{CH_4} \cdot K_{CH_4} + p_{H_2O} \cdot K_{H_2O}\right)^2} \tag{7}$$

The kinetic expressions, in Eqs. (6)-(7), can be compared to the equilibrium approach in Eq. (8) [13]:

$$r_{r,eq} = k \cdot p_{CH_4} \cdot p_{H_2O} \cdot \left(1 - \frac{p_{CO} \cdot p_{H_2}^3}{K_{e,STR} \cdot p_{CH_4} \cdot p_{H_2O}}\right) \tag{8}$$

where K_e is the equilibrium constant. The reaction orders in Eq. (8) are the same as the molar proportions for the respective gas species in the global chemical reaction (1 for both methane and water for the forward reaction, and 3 for hydrogen and 1 for carbon monoxide for the backward reaction).

Different approaches for defining the water-gas shift reaction (Eq. (5)) can be found in literature:

- Global catalytic reaction mechanism that considers reaction in the anode only [18-19].
- Global catalytic reaction mechanism that considers reaction in the anode and gas reaction in the fuel channel [12,15].
- A more advanced reaction mechanism that includes the catalytic surface reaction kinetics for the steam reforming, water-gas shift and the Boudouard reactions can be found in [20-21], among others.

It is frequently stated in literature [12,15] that the water-gas shift reaction should be considered to be in (or very close to) equilibrium state. Equilibrium can be assumed since this reaction is very fast under the conditions found within a SOFC. When the equilibrium is assumed the reaction speed

can be expressed with an equilibrium-limited shift reaction rate expression, first order in carbon monoxide as [22]:

$$r_s = k_s \cdot p_{CO} \cdot \left(1 - \frac{p_{CO_2} \cdot p_{H_2}}{K_{e,s} \cdot p_{CO} \cdot p_{H_2O}} \right) \tag{9}$$

where r_s is the reaction speed of the water-gas shift reaction, k_s the pre-exponential factor, p_i partial pressure for the respective species and $K_{e,s}$ the temperature dependent equilibrium constant.

4 Elementary surface reactions kinetics

Elementary-kinetic electrochemical reactions in the SOFC electrodes are strongly connected to the heterogeneous catalysis and the surface chemistry. Note that information considering the surface coverages of intermediate species are not available when the global approach is applied. Both for the anode and cathode there is a disagreement considering the involved reaction pathways, rate-limiting steps and intermediate species [23-24]. Elementary-kinetic models are normally limited to only the electroactive region, and couplings to transport models are still rare. The surface coverage can be calculated with for example a mean-field approach, where it is assumed that the surface state can be described with average quantities, such as surface coverage, thermodynamic and kinetic adsorbate properties. The composition (segregation phenomena and impurities) and the detailed surface structure (steps, edges and terraces), evaluated at atomic scales, are then not further resolved, when using the mean-field approach. The surface concentration of the different species is then normalized to the total concentration of available surface sites, yielding the dimensionless coverage. The surface species are coupled to the gas-phase species via desorption and adsorption reactions, and to bulk-phase species via surface/bulk exchange reactions. The surface species are also participating in these reactions among themselves [23].

A thermodynamic analysis can be performed to observed trends in reforming reactivity of different metals. Jones et al. [25] investigates suitable catalysts for the methane steam reforming. Au, Ag, Cu, Pt, Pd, Ni, Co, Ru and W are included in the concerned analysis. All of these metals are counted as transition elements in the periodic table (previously named d-block). Potential metals are excluded stepwise:

- An overall energy diagram tells that the noble metals (Au, Ag and Cu) are unsuitable for steam reforming reaction, since the first 6 steps of the reactions, all the way from $CH_4(g)$ + $H_2O(g)$ to C* + O*, are significantly uphill energetically.
- It is also concluded that W binds C* and O* very strongly, and the further reaction is unlikely to appear.
- In terms of the free energy profiles of the reaction, Pt and Pd are found to be unfavorable for the adsorption and desorption of molecular water.
- A possibility of poisoning effects appears, for example for Co, where O* and OH* are adsorbed more strongly, compared to the other investigated metals.

This simple investigation revealed that Ni and Ru might be suitable for the catalytic methane steam reforming reaction [25]. SOFCs contain in general a porous Ni/YSZ structure in the anodes, which enables the electrochemical reactions at the TPB at the anode/electrolyte interface [1]. It can be concluded that Ni is a good choice as catalytic material in the anodes, due to its low cost and possibility for both the electrochemical reactions and also the steam reforming reactions.

4.1 Different pathways for the catalytic methane steam reforming reaction

Knowledge of the catalytic reaction mechanism considering steam reforming of hydrocarbons is counted as a key importance for designing an anode material with a high efficiency and a long life length [26]. The CO* formation as well as the CH_4(g) adsorption have been suggested as rate limiting steps. According to Jones et al. [25] the rate limiting step changes from CO* formation to CH_4(g) adsorption as the temperature is increased.

The conception with rate limiting steps describes phenomena occurring at the microscopic scale, to be compared to the equilibrium constants at the macroscopic scale. Le Chatelier's principle tells that the equilibrium constant for the steam reforming reaction increases as the temperature is increased, since this reaction is endothermic. An increased equilibrium constant means that the equilibrium proceeds further to the right. The water-gas shift reaction is exothermic and its equilibrium constant decreases as the temperature is increased. An increased pressure causes the equilibrium shifting to the side with fewer moles of gas, i.e. the equilibrium constant is decreased for the steam reforming reaction. For the water-gas shift reaction the pressure have no effect on the equilibrium constant. Note that the steam reforming reaction does normally not reach equilibrium conditions within a SOFC, compared to the water-gas shift reaction that is normally assumed to be in equilibrium.

A multi-step heterogeneous reaction mechanism (HCR) for Ni/YSZ catalysts has been developed by [27]. This mechanism consists of 21 reversible reactions, 6 gas-phase species and 12 surface adsorbed species. The mechanism is elementary in nature and covers the global aspects of the reforming, the water-gas shift, the Bouduard reactions and also the surface-carbon coverage. A simplified sketch of this reaction mechanism can be seen in Fig. 1. Most of the expressions are expressed in the Arrhenius rate form and are dependent on the surface coverage. This model is validated by the experimental results. The experiments (using a porous Ni-YSZ anode) were designed to measure the extent of reformation processes under the conditions well away from equilibrium conditions. Pure steam reforming and pure dry reforming with carbon dioxide as well as a combination of these were included in the validation. Note that this mechanism is not validated on the conditions where coking and bulk-phase Ni oxidation occur [27].

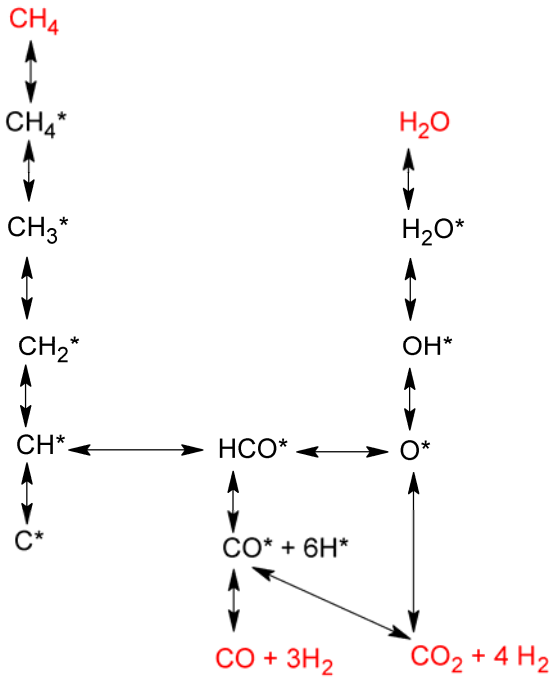

Figure 1. Simplified sketch of the catalytic reforming reaction mechanism proposed by Hecht et al. [27] and Janardhanan and Deutschmann [20] among others. Note that the generation and consumption of H, O* and OH* in each reaction step is not explicitly shown in the figure. The gas reactants and products are marked with red color.*

The HCR developed by [27] was extended by [20] to describe a larger temperature range between 220 and 1700 °C (compared to a constant temperature of 800 °C). However the same chemical reaction schemes were included.

Hofmann et al. [21] compared the HCR from [20] with a simplified approach, where the methane reforming is described by a global kinetic approach and the water-gas shift reaction is in equilibrium. The HCR model can be used to calculate the catalytic surface coverage. It is concluded that the HCR predicts a less steep methane consumption along the flow channel. Slower methane conversion means less hydrogen available throughout the cell. Also the temperature distribution is significantly affected by the steam reforming reaction, with a flatter temperature gradient by the HCR model compared to that by a global approach.

Blaylock et al. [28] investigated different reaction pathways and kinetics of the methane steam reforming reaction over the Ni(111) surfaces, in order to develop a comprehensive ab initio microkinetic model. The Ni(111) surface is sometimes also referred as Ni terrace, known to be catalytically active, and it is the most stable facet on Ni crystallites. The reaction scheme consists of 7 gas-phase species, 18 surface adsorbed species and 36 reversible reactions. A simplified sketch of this reaction scheme can be found in Fig. 2. Besides the Ni terrace also the step sites catalyze the methane steam reforming reaction, i.e. a model that considers only the Ni terrace underestimates the reaction rate.

The reaction mechanism from [27] in Fig. 1 and the one from [28] in Fig. 2 differ concerning the amount of intermediate adsorbed surface species included. The later approach with a larger amount of adsorbed surface species contains obviously a lager amount of reaction steps. For instance, the first reaction step in Hecht et al. contains the adsorption of CH_4(g) to CH_4*, compared to the adsorption of CH_4(g) to CH_3* + H* in [28]. It should be noted that [28] also include more intermediate gas species, i.e. CH_2O and CH_3OH (not shown in Fig. 2).

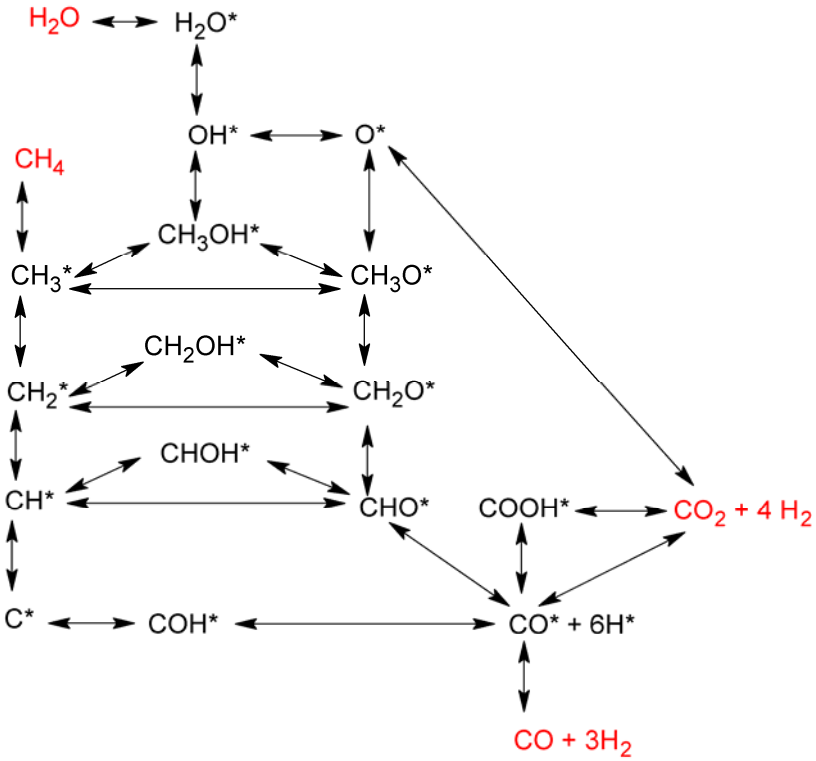

Figure 2. Simplified sketch of the catalytic reforming reaction mechanism proposed by Blaylock et al. [28]. Note that the generation and consumption of H, O* and OH* in each reaction step is not explicitly shown in the figure. The gas reactants and products are marked with red color.*

Density functional theory (DFT) calculations are performed to investigate the thermo-chemistry of the methane steam reforming. It is found that cleaving of a C-H bond is in general predicted to have a smaller barrier than cleavage of a O-H bond, on the Ni(111) surface. The oxygen addition as well as hydroxyl addition reactions are predicted to have higher barriers, compared to the dehydrogenation reactions. It is concluded that it is easier to remove an atom of hydrogen, compared to the one of oxygen, from carbon, i.e. the probability that CH_xOH will form $CH_{(x-1)}OH$ is higher than for CH_xO. The reactions occurring from the adsorption of $CH_4(g)$ until the formation of CH* occurs relatively smoothly [28]. Vang et al. [29] point out that the bond breaking selectivity on the different catalytic sites determines the selectivity that can be observed on the macroscopic scale. It is found that C-C bond breaking can be prevented by blocking the step sites, instead the breaking of C-H bonds will be more significant.

For the case in [28] 87% of the total reaction flux is predicted to involve the reaction of CH* with one oxygen containing species. CHO* is formed from CH* and O*, and decomposed later to form CO* and H*. This single reaction path corresponds to approximately 56% of the total reaction flux. The formation of CHOH* from OH* and CH*, with a subsequent reaction to COH*, is the second-most-active pathway and corresponds to 31% of the total reaction flux. The reaction of CH_2* with either OH* or O* involves 12% of the total flux.

It can be seen in Table 1 that three surface species, H*, CO* and O*, make up most of the predicted surface coverages, as revealed in the open literature. It should be noted that empty Ni surfaces occupy more than half of the available surface sites. It is found that the surface coverage depends on the current density, gas species concentration, temperature and the location within the anode. Blaylock et al. [28] include additional surface species, as follows in the order of decreasing

surface coverages: H_2O*, CO_2*, CH*, OH*, CH_2*, C*, COH*, CH_3*, CHO*, CH_3OH*, CH_3O*, COOH*, CHOH*, CH_2O*, CH_2OH*.

A higher fraction of H_2O in the fuel mixture gives a higher coverage of H*, but a lower of CO*. As the current density increases the surface fraction of empty sites increases, but the coverages of H* and CO* decrease [20]. The coverage of O* reaches its highest values close to the TPB, but for H* the opposite situation appears, as hydrogen is consumed at the TPB. The CO* coverage has it's maximum value in the middle (considering thickness) of the anode and the fraction of empty surface sites reaches it's minimum value in the same area [27]. An increased temperature increase the fraction of empty Ni sites and decrease the surface coverages of CO*, H* and O* [30].

Table 1. Surface coverage when methane reforming reaction is applied in SOFCs.

The steam reforming reactions have at least two kinds of active catalytic sites on Ni, the very active one associated with step and defect sites on the surface and the less active one associated with the close-packed facets. It is found that there are at least two different reaction channels for the steam reforming of methane on Ni, the one associated with steps with a low activation barrier and one associated with terraces with a higher activation barrier. It is concluded that there is many more active terrace sites compared to active step sites. The graphite formation occurs at the step sites. It is possible to add different additives that block different step sites and certainly decreases the probability for graphite formation. An optimized catalyst will have just enough additives that graphite formation is effectively blocked, while the fast channel reaction can still proceed [31].

Metal particles grown at high temperature on graphite or oxide substrate have polyhedral shapes exhibiting (111), (100) and (110) facets. Ni(111) is frequently included in kinetic and thermodynamic studies, but Ni(100) and Ni(110) are less studied. Wang et al. [32] use a density functional theory approach to investigate and clarify the thermodynamics of CH_4 dissociation on Ni-based catalysts:

Ni(111) has 4 possible surface sites: the top site (tp), the bridge site (br), the hexagonal-closed-packed site (hcp) and the face-centered cubic site (fcc). Stable structures are found for CH_3* (tp-a1, tp-a2, hcp-c and fcc-d), CH_2* (tp-a, hcp-c and fcc-d), CH* (hcp-c and fcc-d), C* (hcp-c and fcc-d) and H* (tp-a, hcp-c and fcc-d). On the basis of the binding energy it is found that CH_x and H prefer to chemisorb on the hcp and fcc [32].

Ni(100) has 3 possible surface sites: the tp, the br, and the hollow site (hl). Stable structures are found for CH_3* (tp-e1, tp-e2, br-f1 and br-f2), CH_2* (tp-e1, tp-e2, br-f and hl-g), CH* (hl-g), C* (hl-g) and H* (tp-e, br-f and hl-g). On the basis of the binding energy it is concluded that CH_3 prefer to chemisorb on the br, while CH_2, CH, C and H prefer to chemisorb on the hl. It is further concluded that Ni(100) has a high reactivity, but a low stability as catalyst for CH_4 reforming reactions [32].

Ni(110) has 6 possible surface sites: the top-up site (tu), the short bridge site (sb), the top-down site (td), the long-bridge site (lb), the hollow site formed by two top-layers Ni and one sub-layer Ni (u2dl) and the hollow site formed by one lop-layer Ni and two sub-layers Ni (uld2). Stable structures are found for CH_3* (tu-h1, tu-h2, sb-i1 and sb-i2), CH_2* (tu-h, sb-I and td-j), CH* (sp-I, usdl-l, lb-k and td-j), C* (tu-h, sb-i, lb-k, td-j) and H* (tu-h, sb-I, u2dl-l and lb-k). On the basis of the binding energy it is found that CH_3 and CH_2 prefer to chemisorb on the sb, while CH, C and H prefer to chemisorb on the lb, td and u2dl, respectively [32].

4.2 Microkinetic models

A great deal of information is available for Ni as reforming catalyst, because it has been commonly used for catalysis in the chemical industry. For SOFC anodes the ceramic oxygen-ion conductor YSZ itself also has catalytic activity for partial oxidation. Most reaction rates are represented in an Arrhenius type equation or as a sticking coefficient. A kinetic model can be constructed by combining thermochemical values for each species with computed activation energies and transition-state properties. The forward rate coefficients are described either as a surface reaction rate coefficient or an adsorption reaction. The original kinetic data is often taken from a variety of different catalysis studies which makes the mechanism not thermodynamically consistent. Therefore some of the original kinetic parameters are often modified to ensure the overall consistency concerning the enthalpy and entropy. This approach permits the computation of the reverse reaction rate coefficients, which in turn is dependent on the forward reaction rate coefficients [27]. Since this mechanism is based on the elementary steps, it is therefore represented in all the global processes in the anode.

For the surface reactions and the desorption reactions, often the Arrhenius form is applied for the reaction rate constants, at least for small or moderate variations of the temperature for the reactions [33]. The Arrhenius form is introduced in Eq. (6) for the global reaction kinetics and can be compared to the following equations. The reaction rate constant of a generalized modification of an Arrhenius type equation including the species coverage can be expressed as:

$$k_i = A_i \cdot T^{n_i} \cdot \exp\left(\frac{-E_i}{R \cdot T}\right) \prod_{k=1}^{K_g+K_s} \theta_k^{\mu_{ki}} \cdot \exp\left(\frac{-\varepsilon_{ki} \cdot \theta_k}{R \cdot T}\right) \tag{10}$$

where A_i is the pre-exponential factor, T the reaction temperature, n_i the temperature exponent fraction, R the gas constant and E_i the activation energy for the reaction i. To describe the coverage dependency, μ_{ki} and ε_{ki} are introduced for the parameters for species k and reaction i.

The species molar production rate depends on the surface species concentration which is sometimes expressed as the coverage θ_k. The coverage is the fraction of the surface sites covered by the adsorbed species k to the total active sites on the catalyst surface. The relation between the surface coverage or the surface concentration is expressed as [34]:

$$\theta_k = \frac{c_k \cdot \sigma_k}{\Gamma_{tot}} \tag{11}$$

where θ_k is the surface coverage, σ_k the co-ordination number (number of sites required for a species of adsorption), c_k the concentration and Γ_{tot} the total surface site density.

The reaction rate constant for the surface reaction can also be written as [28]:

$$k_i = \left(\frac{k_b \cdot T}{h}\right) \cdot \left(\frac{Q^{TS} \cdot \left(Q'_{slab}\right)^{R_{tot}-1}}{\prod_{r=1}^{R_{tot}} Q_r}\right) \cdot v \frac{N_{sites}^{0\,R_{tot}-1}}{C_T^{R_{ads}-1}} \cdot \exp\left(\frac{-E_b}{R \cdot T}\right) \tag{12}$$

where k_b is the Boltzmann constant, h the Plank constant, Q the total partition function, R_{tot} the total number of reactants participating in the reaction, R_{ads} the total number of adsorbate reactants and N_{sites} the standard-state number of binding sites per adsorbate.

Non-activated adsorption is calculated using the kinetic theory of the gases assuming the sticking coefficient to be equal to the fraction of vacant sites. The forward reaction rate constant can be presented for the non-activated adsorption as [28]:

$$k_i = \sqrt{\frac{k_b \cdot T}{2 \cdot \pi \cdot M}} \tag{13}$$

where M is the molecular mass of the gas phase species and k_j the reaction rate constant.

Hecht et al. [27], Janharhanen and Deutschmann [20] and Hofmann et al. [21] are, for the adsorption reactions, applying an approach with a sticking coefficient instead of the approach in Eq. 10. The forward reaction rate constants including the sticking coefficient for the non-activated adsorption reaction can be expressed as:

$$k_i = \frac{\gamma_j}{\left(\Gamma_{tot}\right)^m} \cdot \sqrt{\frac{R \cdot T}{2 \cdot \pi \cdot M}} \tag{14}$$

where γ_j is the sticking coefficient

For the activated adsorption and for the surface reactions, the transition-state theory can be applied to obtain the reaction rate coefficients for the forward reaction. The forward reaction rate constant for activated molecular adsorption is written as [28]:

$$k_i = \left(\frac{k_b \cdot T}{h}\right) \cdot \left(\frac{Q^{TS}}{Q_{gas} \cdot Q_{slab}}\right) \cdot \left(\frac{R \cdot T}{p_0}\right) \cdot \Gamma_{tot} \cdot \exp\left(\frac{-E_b}{R \cdot T}\right) \tag{15}$$

where E_b is the classical electronic energy barrier of adsorption and p_0 the standard pressure.

The construction of a kinetic model for the relationship between the standard free energy change of an elementary reaction step and the equilibrium constant needs to be formed. When the equilibrium constant and the forward reaction rate constant are known, the reverse reaction rate constant can be expressed as [35]:

$$k_{-1,i} = \frac{k_i}{K_{e,i}} \tag{16}$$

where $K_{e,j}$ is the equilibrium constant. The equilibrium constant of a reaction can be defined as [33]:

$$K_{e,j} = \exp\left(-\frac{\Delta G_i}{R \cdot T}\right) = \exp\left(-\frac{\Delta H_i - T \cdot \Delta S_i}{R \cdot T}\right) \tag{17}$$

where ΔG is the change in Gibbs energy due to chemical reaction, ΔH is the enthalpy change of the reaction and ΔS the entropy change of the reaction. It should be noted that the principle of reversibility should be used with some caution. The mechanism for the reaction can be reversible for a given set of concentrations, temperature and pressure, but may not be valid for different sets of reaction conditions. The reaction may proceed through the same steps in the forward and the backward reactions but the rate of the individual steps may differ by several orders of magnitude [33].

5 Conclusions

Understanding of the methane steam reforming reactions is expected to be of significant importance for the further SOFC development. The reforming reaction rates are either described by a global kinetics approach or by a more detailed approach applying elementary surface reaction kinetics. It is concluded that the reaction order varies significantly in the global models. The reaction order for water can be negative or positive. It is found that the water-gas shift reaction is usually assumed to be in equilibrium both in the anode as well as in the fuel channel. Different mechanisms considering elementary surface kinetics have been developed, however there is a disagreement considering the involved reaction pathways, intermediate species and rate-limiting steps. The CO* formation as well as the methane adsorption has been suggested as rate limiting steps. It should be noted that empty nickel occupies normally more than half of the available surfaces, as identified in the open literature. Three surface species (H*, CO* and O*) are dominant components in terms of the surface coverage. The nickel particle surfaces contain variable structures for the catalytic reactions. Typically only parts of them are chemically available. This might be the reason of the lower reaction rate predicted by the detailed models, compared to those by the global models.

6 Acknowledgement

The financial support from the Swedish Research Council (VR) and the European Research Council (ERC) is gratefully acknowledged.

7 Nomenclature

c_k	concentration, mol/m^2
E	activation energy, kJ/mol
E_b	classical electronic energy barrier of adsorption, J/mol
ΔG	Gibbs energy, J/mol
h	Plank constant, J·s
ΔH	enthalpy change of reaction, J/mol
k	reaction rate constant, mol/(m^3·Pa^2·s)
k_b	Boltzmann constant, 1.38 ·10^{-23} J/K
K_e	equilibrium constant, unit depends on the actual reaction
M	molecular mass, kg/mol
N_{sites}	standard-state number of binding sites per adsorbate.
p	pressure, Pa, bar
Q	total partition function
r	chemical reaction rate, mol/(m^3·s), mol/(m^2·s)
R	gas constant, 8.314 J/(mol·K)
R_{ads}	total number of adsorbate reactants
R_{tot}	total number of reactants participating in the reaction,
SA	surface area ratio, m^2/m^3
ΔS	entropy change of reaction, J/(mol·K)
T	temperature, K

7.1 Greek symbols

σ_k	co-ordination number, mol/m^2
θ_k	surface coverage, -
γ_j	sticking coefficient, -
Γ_{tot}	surface site density, mol/m^2

7.2 Abbreviations

DFT	density functional theory
DIR	direct internal reforming
ER	external reforming
FC	fuel cell

g	gas phase
HCR	heterogeneous reaction mechanism
HT	high temperature
IIR	indirect internal reforming
IR	internal reforming
IT	intermediate temperature
LT	low temperature
PEMFC	proton exchange membrane fuel cell
SC	steam-to-carbon ratio
SOFC	solid oxide fuel cell
TPB	three-phase boundary
YSZ	yttria-stabilized zirconia

7.3 Chemical

*	surface species connected to the catalytic (Ni) active area
Ag	silver
Au	gold
CH_4	methane
CO	carbon monoxide
Co	cobalt
CO_2	carbon dioxide
Cu	copper
H_2	hydrogen
H_2O	water
Ni	nickel
O_2	oxygen
Pd	palladium
Pt	platinum
Ru	ruthenium
W	tungsten

7.4 Facets on Ni

br	bridge site, on Ni(111) and Ni(100)
fcc	face-centered cubic site, on Ni(111)
hcp	hexagonal-closed-packed site, on Ni(111)
hl	hollow site, on Ni(111)
lb	long-bridge site, on Ni(110)
sb	short bridge site, on Ni(110)
td	top-down site, on Ni(110)
tp	top site, on Ni(111) and Ni(100)
tu	top-up site, on Ni(110)
u2dl	hollow site formed by two top-layers Ni and one sub-layer Ni, on Ni(110)
uld2	hollow site formed by one lop-layer Ni and two sub-layers Ni, on Ni(110)

Table 1. Surface coverage when methane reforming reaction is applied in SOFCs.

	Blaylock *et al.* [28]	**Janardhanan and Deutschmann [20]** [1]	**Hecht *et al.* [27]** [2]	**Hofmann *et al.* [21]** [3]	**Li *et al.* [30]** [4]	**Li *et al.* [30]** [5]
Ni	0.77	0.58-0.66	0.60-0.70	0.76-0.77	0.4-0.6	0.57-0.73
H*	0.15	0.10-0.15	0.05-0.12	0.05-0.07	0.13-0.18	0.12-0.22
CO*	0.077	0.19-0.25	0.10-0.30	0.05-0.11	0.18-0.50	0.12-0.18
O*	$3.5 \cdot 10^{-4}$	n/a	0.00-0.15	0.07-0.11	0.00-0.02	0.01-0.02

[1] Janardhanan and Deutchmann [20] varies the current density to investigate the effect on surface coverage. The values presented in this table correspond to a current density between 10 000 and 22 000 A/m^2 with an inlet molar fractions of H_2O being 0.40 and of CH_4 0.60.

[2] Hecht et al. [27] present the surface coverage as a function of location within the anode.

[3] Hofmann et al. [21] vary inlet conditions, according to findings in literature.

[4] Li et al. [30] keep the inlet temperature at 800 °C, for a different current density (between 0 and 10 000 A/m^2).

[5] Li et al. [30] vary the inlet temperature (between 750 and 950 °C), while keep the current density to 10 000 A/m^2.

References

[1] Andersson M, Yuan J, Sundén B. Review on Modeling Development for Multiscale Chemical Reactions Coupled Transport Phenomena in Solid Oxide Fuel Cells, *Applied Energy* 2010; **87** : 1461-1476. DOI: 10.1016/j.apenergy.2009.11.013

[2] Saxe M. Bringing Fuel Cells to Reality and Reality to Fuel Cells, Doctoral Thesis, Department of Chemical Sciences and Engineering, KTH- Royal Institute of Technology, Sweden, 2008.

[3] Kemm M. Dynamic Solid Oxide Fuel Cell Modelling for Non-steady State Simulation of System Applications, Doctoral Thesis, Department of Energy Sciences, Lund University, Sweden, 2006.

[4] Kackac S, Pramuanjaroenkij A, Zhou X. A Review of Numerical Modeling of Solid Oxide Fuel Cells, *I. J. Hydrogen Energy* 2007; **32**:761-786.

[5] Zhu H, Kee R, Janardhanan V, Deutschmann O, Goodwin D. Modeling Elementary Heterogeneous Chemistry and Electrochemistry in Solid-Oxide Fuel Cells, *J. Electrochem. Soc.* 2005; **152**:A2427-A2440.

[6] Ni M, Leung MKH, Leung DYC. Ammonia-Fed Solid Oxide Fuel Cells for Power Generation – A Review, *Int. J. Energy Res* 2009*;* **33**:943-959.

[7] Gooenough JB, Huang Y., Alternative Anode Materials for Solid Oxide Fuel Cells, *J. Power Sources* 2007; **173**:1-10.

[8] Boder M, Dittmeyer R. Catalytic Modification of Conventional SOFC Anodes with a View to Reducing Their Activity for Direct Internal Reforming of Naturalgas, *J. Power Sources* 2006; **155**:13-22.

[9] Dokmaingam P, Assabumrungrat S, Soottitantawat A, Laosiripojana N. Modelling of Tubular-Designed Solid Oxide Fuel Cell with Indirect Internal Reforming Operation Fed by Different Primary Fuels, *J. Power Sources* 2010*;* **195**:69-78

[10] Clarke S, Dicks A, Pointon K, Smith T, Swann A. Catalytic Aspects of the Steam Reforming of Hydrocarbons in Internal Reforming Fuel Cells, *Catalysis Today* 1997; **38**:411-423.

[11] Sadykov VA, Mezentseva NV, Bunina RV, Alikina GM, Lukashevich AI, Kharlamova TS, Rogov VA, Zaikovskii VI, Ishchenko AV, Krieger TA, Bobrenok OF, Smirnova A, Irvine J, Vasylyev OD. Effect of Complex Oxide Promoters and Pd on Activity and Stability of Ni/YSZ (ScSZ) Cermets as Anode Materials for IT SOFC, *Catalysis Today* 2008; **131**:226-237.

[12] Aguiar P, Adjiman CS, Brandon NP. Anode-Supported Intermediate-Temperature Direct Internal Reforming Solid Oxide Fuel Cell II. Model-Based Dynamic Performance and Control, *J. Power Sources* 2005*;***147**:136-147.

[13] Nagel F, Schildhauer T, Biollaz S, Stucki S. Charge, Mass and Heat Transfer Interactions in Solid Oxide Fuel Cells Operated with Different Fuel Gases – a Sensitivity Analysis, *J. Power Sources* 2008; **184**:129–142.

[14] Danilov V.A, M.O. Tade, 2009, A CFD-based model of a planar SOFC for anode flow field design, *Int. J. Hydrogen Energy* 34:8998-9006.

[15] Klein J-M, Bultel Y, Georges S, Pons M. Modeling of a SOFC Fuelled by Methane: From Direct Internal Reforming of Gradual Internal Reforming, *Chem. Eng. Sci.* 2007; **62**:1636–1649.

[16] Marrero-López D, Ruiz-Morales JC, Peña-Martínez J, Canales-Vázquez J, Núñez P. Preparation of Thin Layer Material with Macroporous Microstructure for SOFC Applications, *J. Solid State Chemistry* 2008; **181**:685-692.

[17] Drescher I, Kinetik der Methane-Dampf-Reformierung (in German), Kinetics of the Methane Steam Reforming (title translated to English), 1999, Doctoral Thesis, Research Institute Jülich, Germany

[18] Yuan J, Huang Y, Sundén B, Wang WG. Analysis of Parameter Effects on Chemical Reaction Coupled Transport Phenomena in SOFC Anodes, *Heat and Mass Transfer* 2009; **45**:471-484.

[19] Haberman BA, Young JB. Three-Dimensional Simulation of Chemically Reacting Gas Flows in the Porous Support Structure of an Integrated-Planar Solid Oxide Fuel Cell, *Int. J. Heat and Mass Transfer* 2004; **47**:3617-3629.

[20] Janardhanan VM, Deutschmann O., CFD Analysis of a Solid Oxide Fuel Cell with Internal Reforming: Coupled Interactions of Transport, Heterogeneous Catalysis and Electrochemical Processes, *J. Power Sources* 2006; **162**:1192-1202.

[21] Hofmann P, Panopoulos KD, Fryda LE, Kakaras E. Comparison between Two Methane Reforming Models Applied to a Quasi-Two-Dimensional Planar Solid Oxide Fuel Cell Model, *Energy* 2008; **34**:2151-2157.

[22] Wang L, Zhang H, Weng S. Modeling and Simulation of Solid Oxide Fuel Cell Based on the Volume–Resistance Characteristic Modeling Technique, *J. Power Sources* 2008; **177**:579–589.

[23] Bessler WG, Gewies S, Vogler M. A New Framework for Physically Based Modeling of Solid Oxide Fuel Cells, *Electrochim. Acta* 2007; **53**:1782-1800.

[24] King D, Strohm J, Wang X, Roh H-S, Wang C, Chin Y-H, Wang Y, Lin Y, Rozmiarek R, Singh P. Effect on Nickel Microstructure on Methane Steam Reforming Activity of Ni-YSZ Cermet Anode Catalyst, *J. Catalysis* 2008; **258**:356-365.

[25] Jones G, Jakobsen JG, Shim SS, Kleis J, Andersson MP, Rossmeisl J, Abild-Pedersen F, Bligaard T, Helveg S, Hinnemann B, Rostrup-Nielsen JR, Chorkendorff I, Sehested J, Jens K, Norskov JK. First principles calculations and experimental insight into methane steam reforming over transition metal catalysts, J. Catalysis 2008; **259**:147-160.

[26] Molenda J, Swierczek K, Zajac W. Functional Materials for IT-SOFC, *J. Power Sources* 2007; **173**:657-670.

[27] Hecht E, Gupta G, Zhu H, Dean A, Kee R, Maier L, Deutschmann O. Methane Reforming Kinetics Within a Ni-YSZ SOFC Anode Support, *Applied Catalysis A: General* 2005; **295**:40-51.

[28] Blaylock D, Ogura WT, Green WH, Beran GJO. Computational Investigation of Thermochemistry and Kinetics of Steam Methane Reforming on Ni(111) under Realistic Conditions, *J. Phys. Chem. C* 2009; **113**:4898-4908.

[29] Vang RT, Honkala K, Dahl S, Vestergaard EK, Schnadt J, Lægsgaard E; Clausen BS, Nørskov JK, Besenbacher F, Controlling the Catalytic Bond-Breaking Selectivity of Ni Surfaces by Step Blocking, *Nature Materials* 2005*;* **4**: 160-162.

[30] Li C, Shi Y, Cai N. Elementary Reaction Kinetic Model of an Anode-Supported Solid Oxide Fuel Cell Fueled with Syngas, *J. Power Sources* 2010; **195**:2266-2282.

[31] Bengaard HS, Norskov JK, Sehested J, Clausen BS, Nielsen LP, Molenbroek AM, Rostrup-Nielsen JR. Steam Reforming and Graphite Formation on Ni Catalysts, *J. Catalysis* 2002; **209**:265-384.

[32] Wang S-G, Cao D-B, Li Y-W, Wang J, Jiao H. CH_4 Dissociation on Ni Surfaces: Density Functional Theory Study, *Surface Science* 2006; **600**:3226-3234.

[33] Stolze P. Microkinetic Simulation of Catalytic Reactions, *Progress in Surface Science* 2000;**65**:65-150.

[34] Janardhanan VM, Heuveline V, Deutschmann O., Performance Analysis of a SOFC Under Direct Internal Reforming Conditions, *J. Power Sources* 2007;**172**:296-307.

[35] Yang Y, Du X, Yang L, Huang Y, Xian H. Investigation of Methane Steam Reforming in Planar Porous Support of Solid Oxide Fuel Cell, *App. Therm. Eng.* 2009; **29**:1106-1113.